Industrial Crops and Products 77 (2015) 13–20

Contents lists available at ScienceDirect

Industrial Crops and Products

journal homepage: www.elsevier.com/locate/indcrop

Facile preparation of optically transparent and hydrophobic cellulose nanofibril composite films

Yan Qing[a], Zhiyong Cai[b], Yiqiang Wu[a,*], Chunhua Yao[a,b], Qinglin Wu[a], Xianjun Li[a]

[a] School of Materials Science and Engineering, Central South University of Forestry and Technology, Changsha, Hunan 410004, China
[b] USDA Forest Service, Forest Products Laboratory, Madison, WI 53726-2398, USA

ARTICLE INFO

Article history:
Received 8 April 2015
Received in revised form 20 July 2015
Accepted 8 August 2015

Keywords:
Cellulose nanofibrils
Nanocomposite
Static and dynamic mechanical properties
Visible light transmittance
Wetting and water contact angle

ABSTRACT

Cellulose nanofibril (CNF) and epoxy nanocomposites with high visible light transmittance and low water sensitivity were manufactured by laminating thin layers of epoxy resin onto CNF films prepared through, pressurized filtration in combination with oven drying. Scanning Electron Microscopy (SEM) studies suggest that the resin component bonded to the CNF substrate well. Atomic Force Microscopy (AFM) observation reveals that the resin lamination led to smoother film surface, which helped enhance UV–vis transmittance. The addition of epoxy resin had little effect on the static and dynamic mechanical strength. However, crystalline and interconnected CNFs significantly reduced the loss factor and shifted the glass transition of composite to a high temperature. Compared to pure CNF films, the CNF/epoxy composites showed a 20% improved transparence in the visible light range. The CNF/epoxy composites demonstrated a sufficient water resistance. This composite film could be considered as a potential substrate material in the application of flexible electronics substrates.

1. Introduction

Cellulose is an abundant, self-generating biomass which is created through photosynthesis in trees, bamboo, grass, reeds, and other plants. Cellulose can also be obtained from organic creatures such as crab and bacteria. With an annual production of 1.5×10^{12} tons, cellulose has been considered an inexhaustible and sustainable raw material (Klemm et al., 2005). In particular, recent increase in concerns for environmental protection and sustainability of resources promptes researchers and entrepreneurs to develop and utilize renewable resources. Cellulose nanofibril (CNF), the novel cellulose derivation, was isolated from natural cellulose and successfully produced as early as in 1980s (Herrick et al., 1983; Turbak et al., 1983). The CNF is disintegrated by delamination of pulp fiber into microfibrils and microfibril bundles with nano-scale diameter, under repeated high-shear mechanical homogenization (Herrick et al., 1983; Spence et al., 2010; Zhao et al., 2015), in combination with chemical (Saito et al., 2009), or enzymatic pretreatment (Pääkkö et al., 2007). In addition to the advantages of abundance, renewability, biodegradability, and light weight, CNFs exhibit other impressive features including high aspect ratio, excellent mechanical strength, large surface area, high light transmittance and available surficial groups.

Extensive research has been conducted to design and fabricate neat CNF films and CNF-reinforced biocomposites, which are considered as potential alternatives in the fields of packaging, coating, medical devices, electronics, automation, visual display substrate and filtration (Syverud and Stenius, 2009; Zhu et al., 2014). Similar to the papermaking processes, CNF suspension is filtrated through a membrane (Nakagaito and Yano, 2005; Qing et al., 2015) or casted in a mould (Syverud and Stenius, 2009; Aulin et al., 2010), to remove the excess water and prepare sheets and films. The resultant films, composed of interconnected nanofibrils, forms networks in plane and laminated structure in thickness. This unique morphology offers CNF films with outstanding mechanical strength, high stiffness, improved light transmittance, and high barrier capability to oil and gas. Notably, Fukuzumi et al. (2009) prepared TEMPO-oxidized CNF films, which had tensile stress and elongation of 233 MPa, and 7.6% respectively, while the light transmittance at 600 nm for the films was 90%. Coating 0.4 μm-thickness nanofibrils onto PLA films dramatically decreased the oxygen permeability from 746 to 1 mL m^{-2} day^{-1} Pa^{-1}. For enhancement with crystallinity of nanofibrils, the CNF film is comparable to commercially synthetic polymer (PVdC coated oriented polyester) in oxygen transmission rate, as low as 17 ml m^2 day^{-1} (Syverud and Stenius, 2009). However, because large number of hydrophilic carboxyls are present on the surface of CNFs, neat dry CNF films are sensitive

* Corresponding author. Tel.: +86 731 85623301; fax: +86 731 85623301.
E-mail addresses: wuyq0506@126.com, wuyiqiang@csuft.edu.cn (Y. Wu).

http://dx.doi.org/10.1016/j.indcrop.2015.08.016
0926-6690/

to moisture. The absorption of moisture reduces the intermolecular interactions between CNFs, resulting in thickness swelling, reduced strength and stiffness, and accelerated air permeability (Aulin et al., 2010). This factor has become the major obstacle restricting CNF films from utilization in packaging, conductor substrates, electronics and displays.

Many efforts have been devoted to overcome the drawback of moisture sensitivity of CNF films. Surface silylation (Andresen et al., 2006; Lu et al., 2008; Galland et al., 2014) and acetylation (Tingaut et al., 2010; Cunha et al., 2014) modification convert the hydrophilic groups on CNFs into hydrophobic ones, which decreases surface energy and wettability. Nevertheless, chemical treatment is a complex process and hydrophobic fibrils may have a negative influence on the formation of hydrogen bonds, leading to low mechanical strength. Another approach is to impregnate water-based resin into CNF films (Nakagaito and Yano, 2005; Henriksson and Berglund, 2007), or mixing the resins with CNF suspensions. Thermosetting resins such as phenol formaldehyde (PF) and melamine formaldehyde (MF) well dispersed among CNFs restrains moisture absorption and thickness swelling. However, the dark color of the CNF/PF systems and brittle characteristics of CNF/MF films are the primary disadvantages. Furthermore, the film preparation process of such approaches is time consuming, usually taking 3–4 days to prepare one film. It is still challenging to better disperse hydrophilic fibrils into nonpolar polymers.The nanocomposites produced from CNF reinforced hydrophobic polymers can eventually exhibit improved moisture resistance.

Epoxy is a hydrophobic resin widely used in coatings, adhesives, composites and construction. Works has been reported in recent literature regarding the preparation of CNF/epoxy composites (Lu et al., 2008; Omrani et al., 2008; Tang and Weder, 2010; Liao et al., 2012). CNF/epoxy nanocomposites exhibited high thermal conductivity and low thermal expansion with a resin content of 42 wt% (Shimazaki et al., 2007). The introduction of nanofibers had little effect on the light transparence of CNF/epoxy composites. However, to better disperse CNFs and improve interfacial adhesion, CNF chemical modification (Lu et al., 2008; Tang and Weder, 2010), electrospinning, and other techniques (Liao et al., 2012) are required. In present work, we reported a commercially feasible approach to prepare flexible, transparent, and water-resistant CNF/epoxy nanocomposites through, coating epoxy resin directly onto dry TEMPO oxidized CNF film. The objective of the study was to systematically characterize the composite morphology, mechanical strength, UV–vis transmittance and hygroscopic property. The long-term goal of the current research is to develop basic technology for manufacturing and characterizing of multilayer CNF/epoxy composites.

2. Experimental

2.1. Materials

The 2,2,6,6-tetramethylpiperidinyl-1-oxyl (TEMPO) oxidized CNF suspension was prepared according to the work reported by Saito et al (Saito et al., 2009) and is briefly described below. Commercially-supplied bleached eucalyptus pulp was carboxylated in TEMPO/NaClO/$NaClO_2$ oxidation system, using NaBr as catalyst, under neutral condition. The oxidation reaction was performed at a temperature of 60 °C for 48 h. After carboxylation, the oxidized fiber was thoroughly washed in distilled water and then refined in a disperser with further isolation of fibril bundles. The fiber slurry was diluted to facilitate separation of coarse and fine fractions under centrifuging at 12 000 × *g*. The obtained fine fractions were concentrated to a solid content of approximately 0.4% by ultrafiltration. A final fibrillation step was performed using M-110EH-30 microfluidizer (Microfluidics, Newton, MA, USA), where the nanofibril suspension was processed through two 87-μm and 200-μm interaction chambers connected in series.

A standard liquid epoxy resin (D.E.R.™ 331 from Dow Chemical Company (Midland, MI, USA) was mixed with 30wt% of D.E.R.™ 732 (Dow Chemical Company, Midland, MI, USA), which is a flexible and light colored epoxy, principally used as an additive. The resin mixture was cured by adding a proportional amount of agent D.E.H.™ 26 (tetraethylenepentamine) (Dow Chemical Company, Midland, MI, USA). Specific chemical structures for the chemical agents are presented in Fig. 1.

2.2. Preparation of CNF sheet and CNF/epoxy nanocomposite

The preparation of CNF/Epoxy nanocomposites involved two processes: (1) fabrication of dry CNF sheets, and (2) lamination of epoxy onto CNF sheets. A sketch illustration for the process is exhibited in Fig. 2. Briefly, the CNF suspension diluted into 0.2% concentration was filtrated under air pressure of 0.55 MPa for 10 h in a Hazardous Waste Filtration System (YT30 142HW, Millipore Corporation, Billerica, MA, USA) at room temperature. After squeezing out a large portion of water in the slurry, the obtained wet CNF films were set to air dry for 24 h and then oven dry for an additional 8 h under a load of approximately 250 N. A more detailed explanation of the drying method was also provided in our previous study (Qing et al., 2015). The dried CNF films were then equilibrated in a 50% RH chamber at 27 °C for at least 24 h to release the residual stress and balance the moisture distribution in films.

Predetermined mixtures of epoxy resin and curing agent were manually stirred for 10 min, then left unstirred for 30 min to eliminate bubbles derived from chemical reaction and then uniformly coated on both sides of CNF films. After air curing for 2 min, the epoxy-coated films were sandwiched between two polyethylene terephthalate (PET) plate. A 5 kg steel cylinder roller was moved across the top PET plate to ensure tight contact between resin and plates. The assembly was subsequently placed between two steel plates and cured at room temperature with a pressure of 0.1 MPa for 24 h. The resultant CNF/Epoxy composite films were simply peeled from the polymer plates and were aged at room temperature for more than a week. Finally, 113 μm thick CNF films were coated with resin layers of approximately 10 μm and 19 μm on both sides, which had epoxy resin content of 8.8 wt% and 19.2 wt%, respectively. The composite films were designated as CNF/8.8%Epoxy and CNF/19.2%Epoxy, respectively.

2.3. Characterization

2.3.1. Tensile properties

The tensile properties of CNF and CNF/Epoxy composites were tested using an Instron 5865 universal material testing apparatus (Instron Engineering Corporation, Norwood, MA, USA) with a 500 N load cell, according to ASTM D638-10. The specimens were cut to conform to ASTM D638-10 type V dogbone shape using a die (Qualitest, Tallahassee, FL, USA), and then conditioned at 50% RH and 23 °C for 1 week. The Instron tests were conducted at a crosshead speed of 1 mm/min with a pre-load of 5 N to remove slack. At least 5 specimens were tested for each condition. An approximate 8 mm gage length was marked with two small pieces of electrician tape wrapped in the middle narrow section. A LX 500 laser extensometer (MTS Systems Corporation, Eden Prairie, MN, USA) was used to determine the displacement with sampling frequency of 10 Hz. Strain was calculated from the determined extension and initial gage length. The toughness was calculated by numerical integration of the stress–strain curve. Modulus of elasticity was calculated as the slope of the stress–strain curve in the stress region of 30–70 MPa. Film densities were calculated gravimetrically by

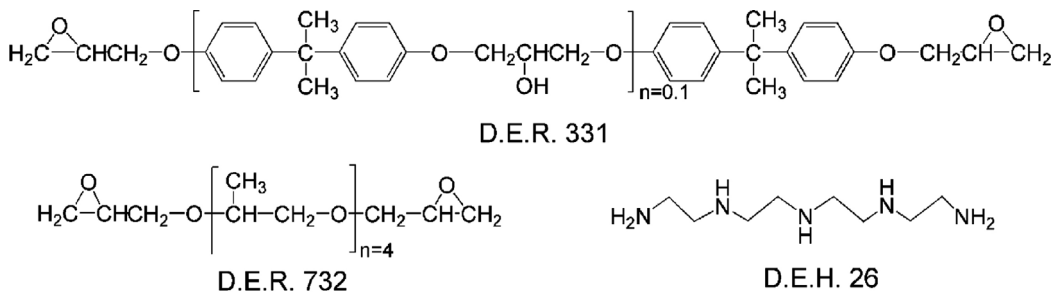

Fig. 1. Chemical structures of epoxies and their curing agent.

measuring the dimensions and weight of multiple well-defined sections of each film.

2.3.2. Dynamic mechanical properties

The test of dynamic mechanical properties for CNF and CNF/Epoxy composites were performed by a film/fiber tension clamps mode on the Q800 DMTA (TA-Instrument, New Castle, DE, USA). Rectangular specimens (30 mm length × 6 mm width) were stocked in a desiccator with dry allochroic silicagel for 2 weeks to remove the free water without violent heating and undesired interactions. The dried specimens were subsequently cooled to 20 °C by liquid nitrogen and maintained at that temperature for 10 min. Measurements were conducted at a heating rate of 3 °C/min from initial temperature 20–200 °C with an amplitude of 15 μm at a frequency of 1 Hz. The dynamic mechanical performances were evaluated by the functions of storage modulus (E') and loss factor ($\tan\delta$) as temperature. Each specimen was measured at least twice until little variation exists between two measurements.

2.3.3. Surface and fracture morphology

The surface and fracture surface of neat CNF, epoxy and CNF/Epoxy composite films were observed using a Magellan 400 scanning electron microscope (FEI, Portland, OR, USA). The fracture surface was derived from the samples after tensile tests. The specimens were held under vacuum and coated with a thin layer of iridium (total thickness approximately 0.4 nm) by a sputter coater. Specimens were held on a carbon tape substrate and the SEM images were taken with an accelerating voltage of 1–2 kV.

In order to evaluate surface smoothness, atomic force microscopy (AFM) scans were performed on the surface of CNF and CNF/8.8%Epoxy composite films using a Digital Instruments AFM (Veeco Metrology Group, Fremont, CA, USA) in tapping mode. The scan size was 20 μm × 20 μm at a scan rate of 1 Hz. Small rectangular samples (approximately 8 mm × 8 mm) were affixed to AFM stubs using epoxy resin. At least four different locations on each specimen were scanned and the typical 3D surface plots were obtained. The surface smoothness (R_q: root mean square average, R_a: arithmetic mean value) was automatically calculated on the basis of the obtained AFM images using the system software.

2.3.4. UV–vis light transmittance

The visible light transmittance for CNF and CNF/Epoxy composite films were measured at a wavelength range from 400 to 800 nm by using an U-4100 ultraviolet-visible (UV-vis) spectrometer (Hitachi High Technologies America Inc., Schaumburg, IL, USA). Rectangular specimens of 40 mm × 9 mm (length × width) were placed in a quartz cuvette and measured by placing them 25 cm from the entrance port of the integrating sphere. Prior to the test, the specimens were conditioned at 50% RH and 23 °C for 2 days. Duplicate tests were performed for each sample.

2.3.5. Water contact angle

To evaluate water resistance, the initial and dynamic water contact angle for CNF and CNF/Epoxy composite films were determined by using PG-X Measuring Head contact angle analyzer (The TMI Group of Companies, New Castle, DE, USA) at 50% RH and 23 °C. Prior to testing, the specimens were conditioned in a humidity room at 50% RH and 23 °C for two days. A drop of distilled water (6.5 μl) was pumped out and deposited on the specimen surface and instantly, a series of images were automatically captured by a compact

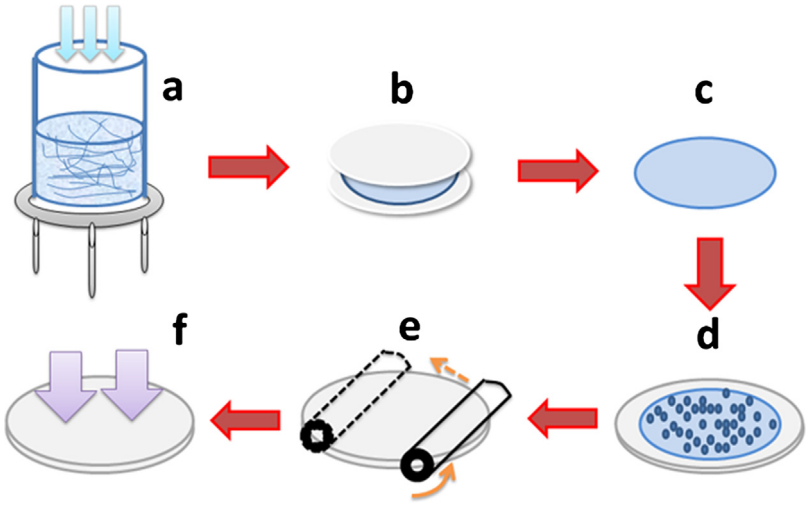

Fig. 2. A procedure for preparing CNF/epoxy biocomposites. (a) Filtration of CNF suspensions under 0.08 MPa air pressure; (b) drying the wet CNF sheets; (c) dry CNF film; (d) coating the epoxy onto both sides of CNF films; (e) rolling-press; (f) curing.

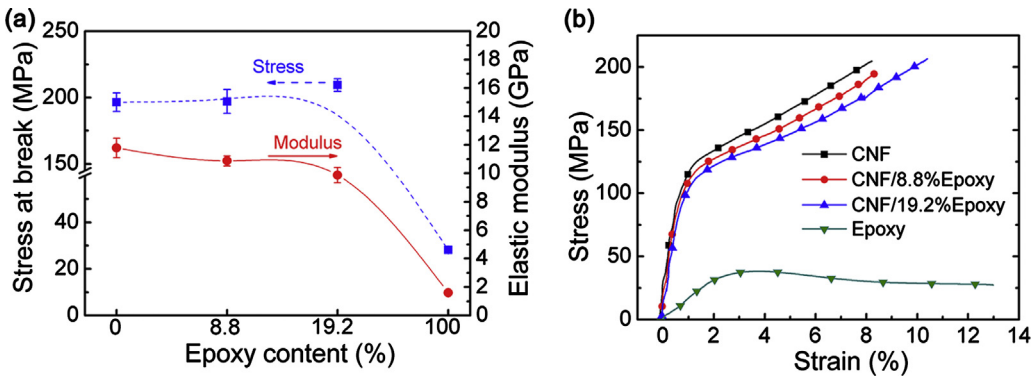

Fig. 3. Tensile properties for CNF and CNF/Epoxy composites, (a) functions of stress at break and modulus as epoxy content, (b) typical stress–strain curves.

camera. The contact angle was calculated by the system software. The dynamic contact angle was measured as a function of time ranging from 0 to 120 s. At least five readings were taken for each condition.

3. Results and discussion

3.1. Mechanical properties

The mechanical properties for CNF/Epoxy compared to neat CNF and epoxy are presented in Fig. 3a, and the representative stress–strain curves are shown in Fig. 3b. Both the CNF films and CNF/Epoxy composites were strong and stiff. The stress of the specimens at breakage ranged from 180 to 230 MPa, and corresponding modulus ranged from 8 to 12 GPa. To the contrary, the neat epoxy is soft and flexible, exhibiting relatively low mechanical strength. The stress at break and modulus for neat epoxy were 30 MPa and 1.6 GPa, respectively. The significant discrepancy was mainly caused by the mechanical properties of CNFs, which exhibited a high theoretical modulus of 150 GPa (Cheng and Wang, 2008). Many attempts have been made using different nanofiber loadings as reinforcing agents to improve epoxy resin (Lu et al., 2008; Tang and Weder, 2010; Liao et al., 2012). The general finding proposed that even with a low nanofiber dosage, the mechanical properties obtained from composites were dramatically increased.

As for the CNF/Epoxy composites, the loading of epoxy had positive effect on stress at break. However, modulus of the composites decreased when epoxy content was increased. This was due to the low modulus of neat epoxy. A similar result was obtained by Nakagatio and Yano (2005). An increase of low-modulus phenol formaldehyde (PF) resulted in a decrease of modulus for the corresponding CNF/PF composites. Additionally, because of low density in neat epoxy (measured approximately 1100 kg/m^3), the density of CNF/Epoxy composites with different epoxy contents was decreased (density of CNF, CNF/8.8%Epoxy, and CNF/19.2%Epoxy are measured 1464, 1424 and1394 kg/m^3, respectively). This was another possible reason explaining the decrease of modulus for CNF/Epoxy composite compared with neat CNF, since the density was an effective indictor in evaluating mechanical properties of polymer-based composites (Takagi and Asano, 2008). However, the stress at break for the CNF/19.2%Epoxy composite was statistically (at $\alpha = 0.05$) higher than the neat CNF films. This was possibly due to the small fraction impregnation of epoxy resin into porous CNF, which had tight adhesion between individual nanofibrils and facilitates stress transfer. This result can also be detected in the dynamic mechanical properties for CNF/8.8%Epoxy composite.

The stress–strain curve for neat epoxy showed a typical mechanical behavior of an amorphous polymer, sustaining remarkable drawing under low stress until broken down. However, the CNF/Epoxy composites followed roughly the same curve but exhibited a decreased yield stress with an increase of epoxy loading. This indicates that thin layer epoxy lamination had little negative effect on the mechanical strength of CNF films, though the epoxy had inferior tensile strength. It in turn provided an alternative in preparing high-performance CNF reinforced composites.

3.2. Dynamic mechanical properties

The dynamic mechanical properties for CNF, CNF/Epoxy composites and epoxy were assessed using Dynamic Mechanical Thermal Analysis (DMTA). Fig. 4a shows the storage modulus (E') and tan δ as functions of temperature ranging from 20 to 200 °C. After holding at 20 °C for 10 min, the E' for neat epoxy was constantly held at 4 GPa until the temperature increased to 28 °C. However, the E' sharply decreased to 180 MPa when the temperature increased to 49 °C, while epoxy underwent a fierce glass-rubber transition reaction. Beyond this temperature, the E' remains constant. Storage modulus lossed of 96% result primarily from the relaxation and mobility of polymer segments during the glass transition (Tang and Weder, 2010; Liao et al., 2012). Compared to neat epoxy, the neat CNF and CNF/Epoxy composite were stiff, which exhibited high E' in the range of 10–13 GPa at 20 °C. The result matched well with static tensile testing at 23 °C. It is interesting to note that the E' of composites incorporating 8.8 wt% epoxy was 2 GPa higher than that of neat CNF. This may contribute to higher pressures used when preparing composites by impregnating more resin into porous network. A similar result was revealed in the composites maximum stress with 19.2 wt% epoxy loading. The storage modulus for neat CNF was gradually decreased by 30% at 200 °C. As for composites, the modulus was radically decreased by 50% when temperature increases to 90 °C, and became stable later. This reinforcement contributed to stiff cellulose crystalline structure and its natural nano network which restricts sharp decreased in storage loss modulus for composites under periodic shear (Svagan et al., 2007).

Fig. 4b depicts the evolution of loss factors (tan δ) for neat CNF, epoxy, and composites as a function of temperature. The neat epoxy showed a mechanical loss factor peak of 0.75 at 50 °C, which corresponds to its glass-rubber transition temperature. Due to different chemical constituents and curing agents, the glass transition temperature for neat PF resin differed dramatically. For instance, Tang and Weder (2010) reported their epoxy resin had transition temperature of 165 °C, Lu et al. (2008) revealed this temperature to be 85 °C, and Liao et al. (2012) proposed this was 40 °C which is similar to the findings in our study. However, the incorporation of CNF definitely resulted in significant decreases of tan δ for composites, and this was confirmed in the above mentioned research. Alternate to reducing its intensity, the addition of CNF into

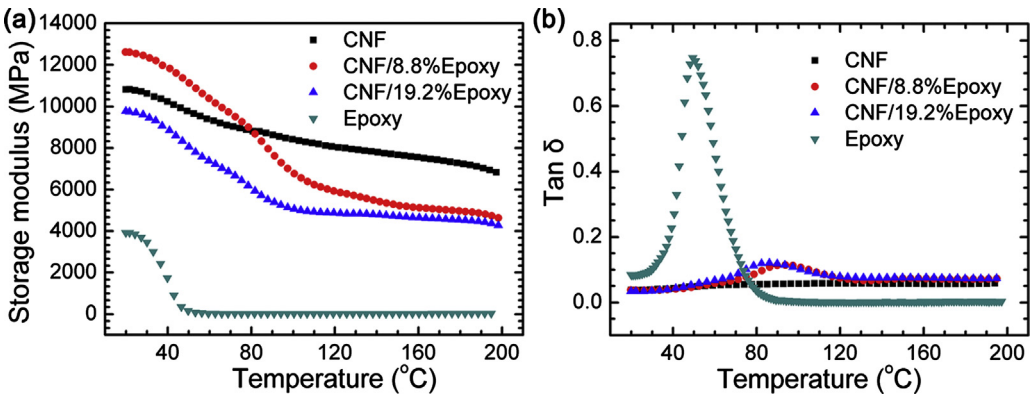

Fig. 4. Storage modulus (a) and tan δ (b) as functions of temperature for neat CNF, epoxy, and CNF/Epoxy composites.

composites obviously shifts tan δ peak to the area of high temperature, depending on the CNF loadings. Similar tan δ behavior was found in other nanofiber reinforced epoxy nanocomposites (Tang and Weder, 2010; Liao et al., 2012). Although huge differences exist between process methods, some resin is deposited on the surface of the CNF assembly. This result indicates that a strong interfacial adhesion was formed between resin and individual nanofibers, as revealed in the static mechanical properties.

3.3. Surficial and fracture morphology

Fig. 5 illustrates the surface and fracture surface morphology of neat CNF and CNF/19.2%Epoxy composite films. Obvious interconnected fibrous networks, composed of uniform nanofibers with diameter ranging 10–15 nm, were portrayed on the surface of neat CNF films. As a comparison, a typical polymer structure with dispersed granular domains showed on the surface of CNF/19.2%Epoxy composite, which was possibly due to fast reaction heat release and original surface morphology of polymer plates.

Regarding fracture surface, smooth fracture surface on the neat CNF films means that the strength of individual nanofibers directly contributes to the mechanical strength of the composites. Another impressive characteristic of layered structure was exhibited in this section. For CNF/19.2%Epoxy composites, a similar fracture surface showed in both the CNF and epoxy regions, even at the interface. The absence of epoxy peeling from the CNF substrate confirms high adhesion between epoxy and nanofibrils. This result indicates the process of epoxy lamination was feasible and reliable. Furthermore, the interface region in Fig. 5e showed epoxy impregnation into porous CNF, which was important in the improvement of above-mentioned mechanical strength and forthcoming light transmittance.

Fig. 6 depicts 3D surface plots for CNF and CNF/8.8Epoxy composite films based on the AFM height images. Though the TEMPO oxidized nanofiber had a diameter less than 15 nm, the surface of the resultant film was little rough. Due to different preparation approaches, the films made from similar nanofibers using solution casting was reportedly smoother (Xhanari et al., 2011). Compared to the neat CNF film, the composite film coated with 8.8% epoxy significant reduced the surface smoothness. The specific Rq and Ra values estimated from the AFM height images for neat CNF are 55.4 ± 10 and 43.5 ± 8 nm, respectively, and are 22.8 ± 5 and 15.2 ± 4 nm for CNF/8.8%Epoxy films, respectively. The surface smoothness for neat CNF film was consistent with results revealed in our previous work. The coating of mobile polymers was found to improve the surface smoothness for cellulose nanofiber films (Couderc et al., 2009; Nogi and Yano, 2009). A possible explanation is that the easy movement of soft polymers helped fill out the voids between nanofibers and the gaps among different bumps. However, the surface morphology for composite film was subsequently determined by the coating plates. As a result, the visible light transmittance benefited from the enhancement of surface smoothness.

3.4. UV–vis light transmittance

High light opacity is one of the promising properties of cellulose nanofibers, which attracts increasing interests. Fig. 7a shows the visible light transmittance for CNF, epoxy and CNF/Epoxy composite films at wavelengths of 300–850 nm. The neat epoxy is typically optically transparent, which performed a 90% light transmittance at wavelengths above 400 nm. On the contrary, the neat CNF film had relative low light transmittance and exhibited an average transmittance of 58% at a wavelength of 600 nm (middle value between 300 and 900 nm). However, by lamination of a very thin layer of transparent epoxy, the light transmittance of CNF/Epoxy composite films was greatly increased to 75% at a wavelength of 600 nm, which was 20% higher compared to neat CNF. Given that materials with more than 80% light transmittance are considered transparent, the CNF/Epoxy composite films ranked among other transparent materials. Additionally, it seems an increase in epoxy loadings did not result in significant improvement of light transmittance. There was little transmittance difference between CNF/8.8%Epoxy and CNF/19.2%Epoxy composite films.

The opacity difference for neat CNF and CNF/Epoxy composite films is presented in Fig. 7b. When viewing objects through films at a distance of approximately 15 cm, clear images can be seen through CNF/Epoxy composite films, while those seen through neat CNF films are obscure and translucent. Since the letters contained in the background image “nofi” are easily seen through both CNF and CNF/Epoxy composite films (shown in Fig. 7c), such differences could be overlooked if the films were placed in close contact with the targeted object.

Due to ultrafine (<100 nm) diameter of nanofibrils, the light scattering of free-standing and condensed CNF film was largely suppressed. The light transmittance was actually used as an effective indicator to assess fibrillation (corresponds linearly with diameter) in the process of nanofiber preparation. Fukuzumi et al. (2009) previously reported the TEMPO films composed of 3–4 nm nanofibrils, showing approximately 90% light transmittance. As for CNF/Epoxy composites, except for ultrafine nanofibers, the smooth surface and small difference in refractive indexes between nanofibers and epoxy resin contribute to increased light transmittance. A similar result was observed by Nogi and Yano (2009), in which translucent CNF sheets were coated with a 10 μm thick layer of transparent acrylic resin. Light transmittance for the obtained sheet increased significantly from 6.1% to 73.4% at a wavelength of 590 nm, because enhancement of surface smoothness by polymer coating resulted

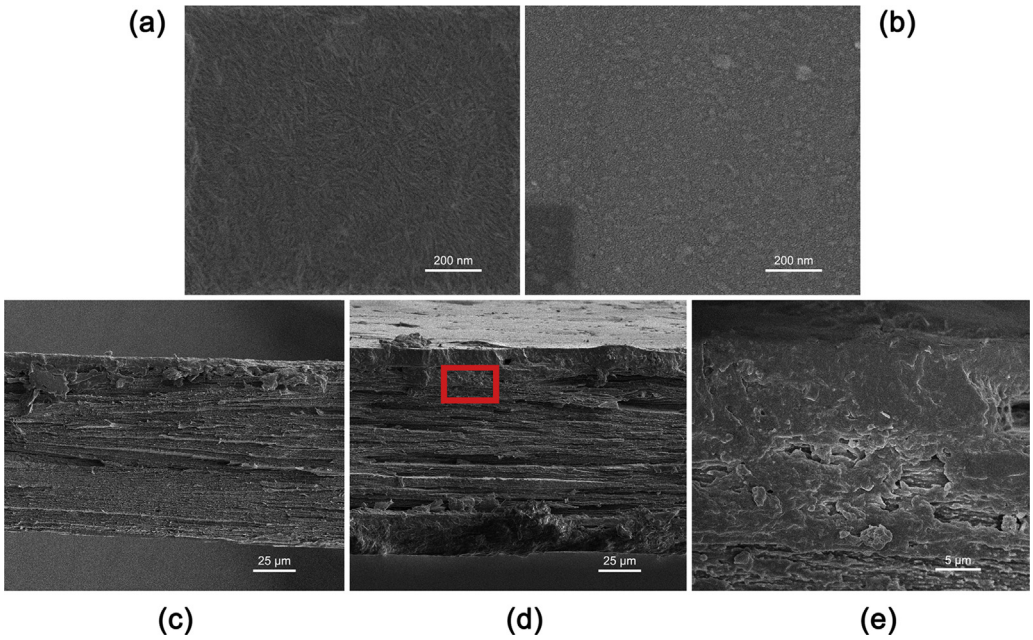

Fig. 5. Surface and fracture SEM images for neat CNF and CNF/19.2%Epoxy composite. (a) and (c) are the surface and fracture images of CNF respectively; (b) and (d) are the corresponding images of CNF/19.2%Epoxy composite; (e) represents marked region with magnified observation.

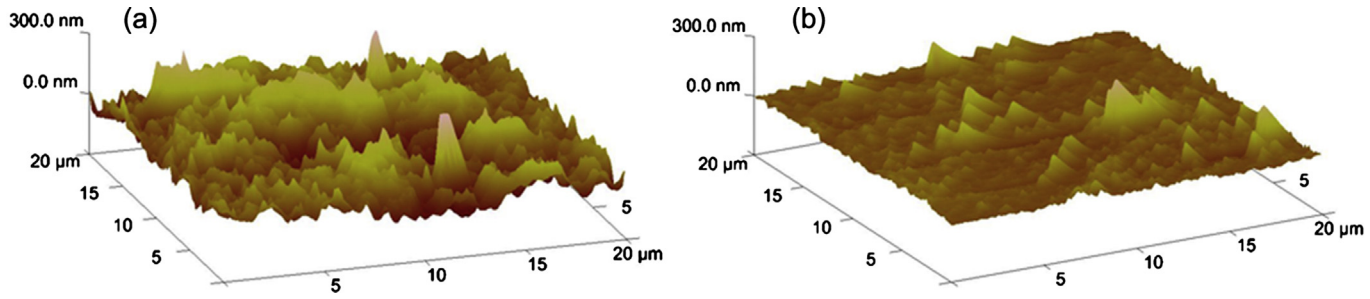

Fig. 6. 3D surface plots of CNF (a) and CNF/8.8%Epoxy (b) composite films.

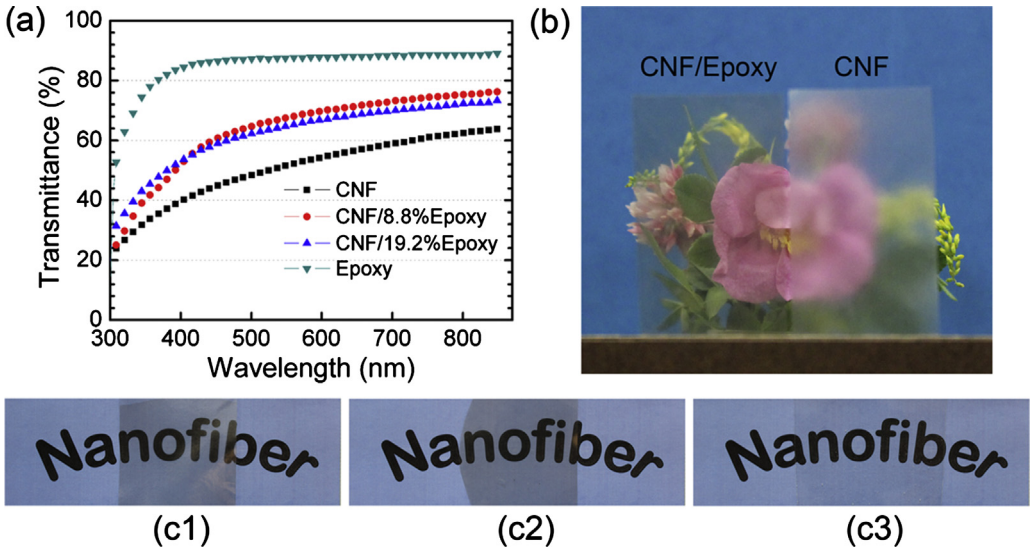

Fig. 7. Visible light transmission performance for neat CNF, epoxy and CNF/Epoxy composites. (a) UV–vis transmission spectra; (b) photographs for CNF and CNF/8.8%Epoxy composite films placed in front of plants; (c) photographs for neat CNF (c1), CNF/19.2%Epoxy composite (c2), and epoxy (c3) films placed on the background paper.

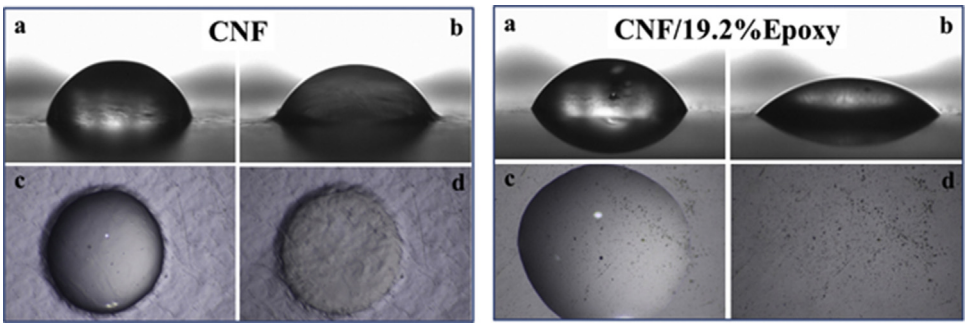

Fig. 8. Shape of water drop (a and b) on the surface of neat CNF and CNF/19.2%Epoxy composite films. (a) is the initial state, and (b) is maintained for 120 s. (c) and (d) are surface photographs for neat CNF and CNF/19.2%Epoxy composite films captured by the optical microscopy, (c) is initial state, (d) is surface after 120 s holding, on which remaining water is taken up by absorbing paper.

Table 1
Initial and dynamic water contact angle of neat CNF, CNF/Epoxy composite, and epoxy films.

Materials	Water contact angle (°)	
	Initial (0.1 s)	120 s later
CNF	70.4 (2.7)	65.1 (1.9)
CNF/8.8%Epoxy	73.9 (2.4)	64.6 (1.8)
CNF/19.2%Epoxy	70.0 (2.2)	42.9 (8.3)
Epoxy	71.3 (3.1)	36.6 (4.8)

in less surface light scattering. It was also observed that mechanical surface polishing of CNF sheets improved their light transmittance. On the other hand, the effect of light reflection would cause great loss of light transmittance when visible light passed through CNF films. Refractive index (RI) values are an effective indicator in comparing light transmittance of materials, where higher RI differences between interfaces leads to higher reflection (Shimazaki et al., 2007; Liao et al., 2012). The nanofibrils and epoxy have RI of 1.54 and 1.62 respectively, compared to RI 1.0 for air (Mark, 2007; Liao et al., 2012). As a result, adhesion between epoxy and nanofibers reduced the interfacial area between nanofibers and air, which helped decrease the RI difference and promote preparation of transparent CNF/Epoxy composites.

3.5. Water contact angle

The abundance of hydrophilic groups on the nanofibrils makes the CNF films sensitive to moisture variation. Exposure of CNF films to high humidity or water resulted in fatal loss of mechanical strength and dimensional stability. Wettability for neat CNF, epoxy and CNF/Epoxy composite films was evaluated by measurement of water contact angle. Of interest, noted in Table 1, neat CNF had an initial water contact angle of 70.4°, which was approximately the same as epoxy, and CNF/Epoxy composites, though epoxy is considered a water-resistant resin. Furthermore, after holding 120 s, the water contact angle for neat CNF was 65.1° which is higher than those on both composites and epoxy. However, this result doesn't mean the neat CNF film is more water-resistant than epoxy and composites. Detailed surface morphology of CNF and CNF/Epoxy composite films (seen in Fig. 8) in initial and final states reveals the real change of water wettability. The images in Fig. 7c and d were captured with an optical microscope equipped with a digital camera at a 40× magnification. Neat CNF films with the water drop maintained on the surface for 120 s show a clear surface bump which leads to relatively high contact angle. In comparison, the surface of CNF/19.2%Epoxy composite film is flat and clear when absorbing the remaining water after 120 s test.

There are large variations of water contact angle data reported for different cellulose nanifibers. For instance, homongenized CNF films present a water contact angle of 28° (Andresen et al., 2006), and lignin as hydrophobic polymer in nanofibers contributes to high water contact angle (Spence et al., 2010). Due to high carboxylate levels on the surface of TEMPO oxidized nanofiber, the resultant films have high water contact angle of 47° (Fukuzumi et al., 2009), which is enhanced along with the increase of carboxylate content (Rodionova et al., 2012). However, no reports recognized the effect of the surface bump on the water contact angle of CNF/resin films. This warrants further study to set up an exact model with which to calculate the accurate water contact angle. Furthermore, the surface of CNF is rougher than epoxy resin, which would result in larger measured water angles due to the formation of air pockets between the rough surface and the droplet (Ryan and Poduska, 2008).

The water contact angle of epoxy is consistent with the result obtained by Yi et al. (2009), in which a similar bisphenol A epoxy was used. Loading of epoxy had little influence on the water contact angle for the resultant composite films, indicating the surface of cellulose nanofibers was thoroughly covered by resin. The decrease of water contact angle for the epoxy and CNF/epoxy composite was caused by the diffusion of water into the polymer surface, evaporation and mobility of water (Shanahan and Bourgès, 1994), because the chemical reaction formed small holes on the surface (seen in Fig. 7c and d for composite films). However, water diffusion and permeation did not result in any bump or distortion on the surface. The results indicated that by coating thin layers of epoxy, the water resistance of CNF films was significantly improved though the surface water contact angle remains unchanged.

Due to the environmental advantages and biodegradability, these obtained CNF/epoxy composite films was successfully applied for the preparation of high-performance green flexible electronics using transfer printing techniques (Jung et al., 2015). It was demonstrated that these green electronics are comparable to the exiting popular electronics such as GaAs-based and Si-based electronics. Concerned with the environmental and economical impact, these nanocomposites are considered as more sustainable, environment-friendly, and green candidate for the advanced electronics and information industry.

4. Conclusions

By laminating a thin epoxy layer onto CNF films, a high-performance CNF/epoxy nanocomposite with high visible light transmittance and low water sensitivity was successfully prepared. The chemical adhesion and impregnation of component epoxy into CNF layers made it strongly bonded to CNF substrates. Lamination of epoxy yielded a smoother composite surface, which helped enhance UV–vis transmittance. The addition of epoxy had little effect on the static and dynamic mechanical strength of CNF films. However, crystalline and interconnected CNFs significantly

reduced the strength loss factor and shifted the glass transition of epoxy to a higher temperature. Compared to neat CNF films, the composites showed 20% improved transparence in the visible light range. Wetting surfaces of the composite did not exhibit any bump compared to neat films, indicating high water resistance. This composite film can be considered a potential material for applications in flexible substrates and barrier packaging.

Acknowledgements

This work was financially supported by Industry Research Special Funds for Public Welfare Project of China (201404604), Hunan Provincial Natural Science Foundation (2015JJ2203), Research Foundation of Education Bureau of Hunan Province (15K151), and Hunan Provincial Innovation Foundation for Postgraduate (CX2014A013) from China. The authors sincerely thank Rick Reiner for preparing and supplying TEMPO oxidized cellulose nanofibrils. The authors gratefully acknowledge Jane O'Dell and Nancy Ross Sutherland for DMTA and water contact angle tests, respectively. Benjamin Treml is kindly acknowledged for help with tensile and UV–vis transmittance tests. Thanks also to Neil Gribbins for technical and editorial assistance.

References

Andresen, M., Johansson, L.S., Tanem, B.S., Stenius, P., 2006. Properties and characterization of hydrophobized microfibrillated cellulose. Cellulose 13, 665–677.
Aulin, C., Gällsted, t, M., Lindström, T., 2010. Oxygen and oil barrier properties of microfibrillated cellulose films and coatings. Cellulose 17, 559–574.
Cheng, Q., Wang, S., 2008. A method for testing the elastic modulus of single cellulose fibrils via atomic force microscopy. Compos. A 39, 1838–1843.
Couderc, S., Ducloux, O., Kim, B.J., Someya, T., 2009. A mechanical switch device made of polyimide-coated microfibrillated cellulose sheet. J. Micromech. Microeng., 19, http://dx.doi.org/10.1088/0960-1317/19/5/055006.
Cunha, A.G., Zhou, Q., Larsson, P.T., Berglund, L.A., 2014. Topochemical acetylation of cellulose nanopaper structures for biocomposites: mechanisms for reduced water vapour sorption. Cellulose 21, 2773–2787.
Fukuzumi, H., Saito, T., Iwata, T., Kumamoto, Y., Isogai, A., 2009. Transparent and high gas barrier films of cellulose nanofibers prepared by TEMPO-mediated oxidation. Biomacromolecules 10, 162–165.
Galland, S., Leterrier, Y., Nardi, T., Plummer, C.J.G., Manson, J.A.E., Berglund, L.A., 2014. UV-cured cellulose nanofiber composites with moisture durable oxygen barrier properties. J. Appl. Polym. Sci. 131, http://dx.doi.org/10.1002/APP.40604.
Henriksson, M., Berglund, L.A., 2007. Structure and properties of cellulose nanocomposite films containing melamine formaldehyde. J. Appl. Polym. Sci. 106, 2817–2824.
Herrick, F.W., Casebier, R.L., Hamilton, J.K., Sandberg, K.R., 1983. Microfibrillated cellulose: morphology and accessibility. J. Appl. Polym. Sci. Appl. Polym. Symp. 37, 797–813.
Jung, Y.H., Chang, T.H., Zhang, H.L., Yao, C.H., Zheng, Q.F., Yang, V.W., Mi, H.Y., Kim, M., Cho, S.J., Park, D.W., Jiang, H., Lee, J., Qiu, Y.J., Zhou, W.D., Cai, Z.Y., Gong, S.Q., Ma, Z.Q., 2015. High-performance green flexible electronics based on biodegradable cellulose nanofibril paper. Nat. Commun. 6, http://dx.doi.org/10.1038/ncomms8170.
Klemm, D., Heublein, B., Fink, H., Bohn, A., 2005. Cellulose: fascinating biopolymer and sustainable raw material. Angew. Chem. Int. Ed. 44, 3358–3393.
Liao, H., Wu, Y., Wu, M., Zhan, X., Liu, H., 2012. Aligned electrospun cellulose fiber reinforced epoxy resin composite films with high visible light transmittance. Cellulose 19, 111–119.
Lu, J., Askeland, P., Drzal, L.T., 2008. Surface modification of microfibrillated cellulose for epoxy composite applications. Polymer 49, 1285–1296.
Mark, J.E. (Ed.), 2007. Physical Properties of Polymers Handbook. , 2nd ed. Springer, New York, pp. 825–850.
Nakagaito, A.N., Yano, H., 2005. Novel high-strength biocomposites based on micro fibrillated cellulose having nano-order-unit web-like network structure. Appl. Phys. A 80, 155–159.
Nogi, M., Yano, H., 2009. Optically transparent nanofiber sheets by deposition of transparent materials: a concept for a roll-to-roll processing. Appl. Phys. Lett. 94, 233117–233119.
Omrani, A., Simon, L.C., Rostami, A.A., 2008. Influences of cellulose nanofiber on the epoxy network formation. Mater. Sci. Eng. A 490, 131–137.
Pääkkö, M., Vapaavuori, J., Silvennoinen, R., Kosonen, H., Ankerfors, M., Lindström, T., Berglund, L.A., Ikkala, O., 2007. Enzymatic hydrolysis combined with mechanical shearing and high-pressure homogenization for nanoscale cellulose fibrils and strong gels. Biomacromolecules 8, 1934–1941.
Qing, Y., Sabo, R., Wu, Y., Zhu, J.Y., Cai, Z., 2015. Self-assembled optically transparent cellulose nanofibril films: effect of nanofibril morphology and drying procedure. Cellulose 22, 1091–1102.
Rodionova, G., Eriksen, Ø., Gregersen, Ø., 2012. TEMPO-oxidized cellulose nanofiber films: effect of surface morphology on water resistance. Cellulose 19, 1115–1123.
Ryan, B.J., Poduska, K.M., 2008. Roughness effect on contact angle measurements. Am. J. Phys. 76, 1074–1077.
Saito, T., Hirota, M., Tamura, N., Kimura, S., Fukuzumi, H., Heux, L., Isogai, A., 2009. Individualization of nano-sized plant cellulose fibrils by direct surface carboxylation using TEMPO catalyst under neutral conditions. Biomacromolecules 10, 1992–1996.
Shanahan, M.E.R., Bourgès, C., 1994. Effect of evaporation on contact angles on polymer surfaces. Int. J. Adhes. Adhes. 14, 201–205.
Shimazaki, Y., Miyazaki, Y., Takezawa, Y., Nogi, M., Abe, K., Ifuku, S., Yano, H., 2007. Excellent thermal conductivity of transparent cellulose nanofiber/epoxy resin nanocomposites. Biomacromolecules 8, 2976–2978.
Spence, K.L., Venditi, R.A., Rojas, O.J., Habibi, Y., Pawlak, J.J., 2010. The effect of chemical composition on microfibrillar cellulose films from wood pulps: water interactions and physical properties for packaging applications. Cellulose 17, 835–848.
Svagan, A.J., Azizi Samir, M.A.S., Berglund, L.A., 2007. Biomimetic polysaccharide nanocomposites of high cellulose content and high toughness. Biomacromolecules 8, 2556–2563.
Syverud, K., Stenius, P., 2009. Strength and barrier properties of MFC films. Cellulose 16, 75–85.
Takagi, H., Asano, A., 2008. Effects of processing conditions on flexural properties of cellulose nanofiber reinforced "green" composites. Compos. A 39, 685–689.
Tang, L., Weder, C., 2010. Cellulose whisker/epoxy resin nanocomposites. ACS Appl. Mater. Interfaces 2, 1073–1080.
Tingaut, P., Zimmermann, T., Lopez-Suevos, F., 2010. Synthesis and characterization of bionancomposites with tunable properties from poly (lactic acid) and acetylated microfibrillated cellulose. Biomacromolecules 11, 545–564.
Turbak, A., Snyder, F.W., Sandberg, K.R., 1983. Microfibrillated cellulose, a new cellulose product: properties, uses, and commercial potential. J. Appl. Polym. Sci. Appl. Polym. Symp. 37, 815–827.
Xhanari, K., Syverud, K., Chinga-Carrasco, G., Paso, K., Stenius, P., 2011. Reduction of water wettability of nanofibrillated cellulose by adsorption of cationic surfactants. Cellulose 18, 257–270.
Yi, F., Zheng, S., Liu, T., 2009. Nanostructures and surface hydrophobicity of self-assembled thermosets involving epoxy resin and poly (2,2,2-trifluoroethyl acrylate)-block-poly(ethylene oxide) amphiphilic diblock copolymer. J. Phys. Chem. B 113, 1857–1868.
Zhao, Y., Xu, C., Xing, C., Shi, X., Matuana, L.M., Zhou, H., Ma, X., 2015. Fabrication and characteristics of cellulose nanofibril films from coconut palm petiole prepared by different mechanical processing. Ind. Crop. Prod. 65, 96–101.
Zhu, H., Fang, Z., Preston, C., Li, Y.Y., Hu, L., 2014. Transparent paper: fabrications, properties, and device applications. Energy Environ. Sci. 7, 269–287.